

π -Junction behavior and Andreev bound states in Kondo quantum dots with superconducting leads

Gabriel Sellier,^{1,2} Thilo Kopp,¹ Johann Kroha,³ and Yuri S. Barash⁴

¹*EP VI, Institut für Physik, Universität Augsburg, 86135 Augsburg, Germany**

²*TKM, Universität Karlsruhe, Postfach 6980, 76128 Karlsruhe, Germany*

³*Physikalisches Institut, Universität Bonn, Nussallee 12, 53115 Bonn, Germany*

⁴*Institute of Solid State Physics, Russian Academy of Sciences, Chernogolovka, 142432 Moscow, Russia*

(Dated: April 2, 2018)

We investigate the temperature- and coupling-dependent transport through Kondo dot contacts with symmetric superconducting s -wave leads. For finite temperature T we use a superconducting extension of a selfconsistent auxiliary boson scheme, termed SNCA, while at $T = 0$ a perturbative renormalization group treatment is applied. The finite-temperature phase diagram for the $0-\pi$ transition of the Josephson current in the junction is established and related to the phase-dependent position of the subgap Kondo resonance with respect to the Fermi energy. The conductance of the contact is evaluated in the zero-bias limit. It approaches zero in the low-temperature regime, however, at finite T its characteristics are changed through the coupling- and temperature-dependent $0-\pi$ transition.

PACS numbers: 74.50.+r, 72.15.Qm

I. INTRODUCTION

The physics of charge and spin transport through Kondo quantum dots is paradigmatic for interface problems with strong correlations mediated by the contact. Novel effects, taking place in junctions with quantum dots between normal metal leads, have been intensively studied for a long period.^{1,2,3,4,5} The Josephson current through a localized spin state was first considered by Shiba and Soda.⁶ Later on Glazman and Matveev investigated more thoroughly the supercurrent through a single resonant state, as well as through a distribution of such impurity states⁷. Eventually, a Kondo quantum dot, which is coupled to a normal and to a superconducting lead, is a further notable system which allows to approach the interplay between Kondo effect and Andreev reflections.^{8,9} The progress in the miniaturization of electronic devices now makes the investigation of electronic transport through a single Kondo impurity technically feasible. To date, several groups have reported on transport measurements of such nanoscale devices^{10,11,12,13,14,15,16}. Besides possible applications as, for example, the study of nonlocal spin-entangled pairs¹⁷, these quantum dot contacts are fascinating on fundamental grounds, because they are the most elementary realization of a “strongly correlated contact”.

From the theoretical side it has been well apprehended that a phase-sensitive subgap state is formed, which is to be interpreted as a Kondo resonance, if the Kondo scale T_K is larger than the gap Δ of the superconducting leads, $T_K/\Delta \gg 1$. Andreev scattering processes induce a dependence of the subgap-state energy on the phase difference ϕ of the superconductors in the leads.¹⁸ The interference of Andreev scattering with Kondo-type spinflip processes leads to a non-trivial behavior of the Josephson current-phase relation $I_s(\phi)$ in Kondo quantum dot junctions. A transition from a 0 -junction to a π -junction

arises on account of the distinct nature of the spin ground states in the strong and in the weak coupling regime. In the strong coupling limit, $T_K/\Delta \gg 1$, the ground state is a spin singlet due to the Kondo screening of the impurity spin, and the Coulomb blockade is lifted by the formation of the Kondo resonance. In this case, coherent Cooper pair transmission occurs without affecting the spin of the electrons in the pair (0 -junction). In the opposite limit of weak coupling, $T_K/\Delta \ll 1$, the Kondo screening is suppressed for temperatures T well below the critical temperature T_c of the superconductors as the Cooper pairs in the bulk cannot be broken for s -wave pairing symmetry. Then the ground state is a Kramers degenerate spin doublet, and a single subgap resonance of width $\sim T_K$ in the impurity spectrum is formed, split off from the continuum spectrum. In this regime, retarded, coherent pair transmission is still possible, but for energetic reasons (no double occupancy of the dot) the temporal sequence of the transmitted electrons with opposite spin is reversed, leading to a π -shift in the current-phase relation (π -junction),¹⁹ see Ref. 20 for a more detailed discussion. Since for weak coupling the subgap state forms below and for strong coupling it moves above the Fermi energy,^{18,21} the current-phase relation $I_s(\phi)$ is also related to the position of the resonance. This behavior of a Kondo quantum dot should be contrasted to the case when the impurity state is not a dynamical quantity and its magnetic moment is fixed. The latter case is analogous to junctions with ferromagnetic interlayers, where Andreev subgap states are generated both below and above the Fermi energy, being split with respect to their spin polarization.^{22,23,24,25}

Whereas the supercurrent through a Kondo correlated junction has been investigated successfully within several approaches, the conductance of the contact is much more difficult to study, as it involves the quasiparticle current. It is essential to distinguish between *Kondo point con-*

tacts and *Kondo quantum dot devices*. A Kondo impurity in a point contact or orifice introduces an additional scattering channel and tends to reduce the transmission similar to the Kondo effect in bulk metals. In contrast, for a Kondo quantum dot device, the quantum dot provides the only transmission channel. For temperatures above T_K and a quantum dot energy level well below the Fermi energy, the transmission channel is “almost closed” as the charge tunneling is suppressed by the Coulomb blockade and because the level is off resonance. Through the formation of the Kondo resonance at temperatures below T_K , on-resonance tunneling enhances the transmission up to the quantum limit.^{3,4,26} While this inverse relation between the two junction types is rather obvious for normal conducting leads, it has more profound consequences in the case of superconductors. In the present paper we study the intrinsic conductance which characterizes the quasiparticle current through Kondo dots between two superconductors. The quasiparticle current is not related in a simple way to the supercurrent and the question arises, if the $0-\pi$ transition may already manifest itself in the zero bias conductance of the Kondo dot contact. Choi *et al.*²⁷ also investigate a Kondo quantum dot with superconducting leads to calculate the Josephson current at $T = 0$. However, to determine the low- T conductance through the $0-\pi$ transition, they consider a Kondo quantum dot with an additional resistive shunting (resistively shunted superconducting junction, RSCJ) in the overdamped regime and compare the crossover for $T_K \approx 0.5\Delta$ with the measured conductance of gated carbon nanotube quantum dots coupled to superconducting Au/Al leads²⁸. Although the RSCJ modelling may well apply to the considered experiments, it actually does not refer to a Kondo quantum dot as defined above. It does not analyze the quasiparticle current through the Kondo impurity but rather the phase slips of the supercurrent. The respective conductance G_S in the RSCJ model grows exponentially with the inverse temperature $G_S/G_N \sim \exp(\hbar I_s/eT)$ where G_N is the conductance in the normal state.

In this article we address two related subjects which are relevant for Kondo dots between two superconducting leads. On the one hand, a finite-temperature phase diagram for the π -junction behavior has not yet been presented. It allows to identify the coupling strength at which the $0-\pi$ transition sets in, but it also renders the regime where the transition may be observed by varying the temperature at fixed coupling strength. On the other hand, we calculate the intrinsic conductance of the Kondo dot contact — a quantity which is not related to the phase difference as directly as the supercurrent. Nevertheless, as both quantities, the supercurrent and the quasiparticle current, are controlled by the position of the subgap resonance, they both display a transition in their dependence on temperature and coupling strength, as we will discuss in this paper. For this investigation we will always consider the generic case of a symmetric junction and s -wave pairing symmetry in the leads.

In Sec. II we briefly introduce the technique used for the Kondo correlated junctions, an extension of the non-crossing approximation (NCA) to the superconducting state (SNCA). Some explicit details about the derivation of the SNCA, its evaluation and regime of validity, as well as the calculation of the supercurrent and the conductance are deferred to the appendices. Sec. III expands the discussion of the $0-\pi$ transition in certain aspects beyond what has been presented in the literature on this topic. Specifically, we focus on the temperature dependence of the transition and introduce a phase diagram. In Sec. IV we address the temperature- and coupling-dependence of the intrinsic conductance of the Kondo dot contact.

II. KONDO IMPURITY BETWEEN TWO SUPERCONDUCTORS

The system of conduction electrons in the left and right lead interacting with a single-channel magnetic impurity or quantum dot is modeled by an infinite- U Anderson Hamiltonian. The s -wave superconducting state in the reservoirs is treated within standard BCS mean-field theory. The complete Hamiltonian then takes the form (see Fig. 1 for a graphical layout of the contact)

$$H = H_0 + H_{BCS} + H_{QD} + \lambda Q \quad (1)$$

with

$$\begin{aligned} H_0 &= \sum_{\mathbf{k}\sigma} \epsilon_{\mathbf{k}} c_{\mathbf{k}\sigma a}^\dagger c_{\mathbf{k}\sigma a}, \\ H_{BCS} &= - \sum_{\mathbf{k}a} \Delta_a \left(c_{\mathbf{k}\uparrow a}^\dagger c_{-\mathbf{k}\downarrow a}^\dagger + \text{h.c.} \right), \\ H_{QD} &= \sum_{\sigma} \epsilon_d f_{\sigma}^\dagger f_{\sigma} + \sum_{\mathbf{k}\sigma} V_a \left(c_{\mathbf{k}\sigma a}^\dagger b^\dagger f_{\sigma} + \text{h.c.} \right). \end{aligned}$$

Here we have adopted a slave-boson representation²⁹ for the dot states, where the local creation and annihilation operators for an electron in the dot (d -) orbital with spin σ and energy ϵ_d are decomposed as, for example, $d_{\sigma}^\dagger = f_{\sigma}^\dagger b$. The operators f_{σ}^\dagger and b^\dagger create a singly occupied or an empty occupied impurity state, whenever an electron hops onto or off the dot, respectively, and obey the canonical fermion and boson commutation relations. Their dynamics are restricted to the physical Hilbert space by the operator constraint

$$Q = \sum_{\sigma} f_{\sigma}^\dagger f_{\sigma} + b^\dagger b = 1, \quad (2)$$

which will be enforced exactly by taking the limit of the parameter $\lambda \rightarrow \infty$ (see Appendix A).³⁰ Moreover, $c_{\mathbf{k}\sigma a}^\dagger$ creates a conduction electron in the left (L) or right (R) superconductor, $a = L, R$. The hybridization of these electronic states in the leads with the quantum dot state is parameterized by V_a . For convenience, we introduce

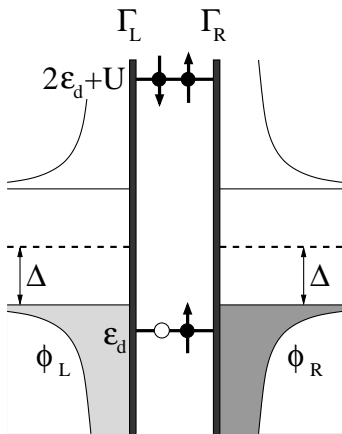


FIG. 1: Quantum dot coupled to two superconductors. Γ_L and Γ_R denote the effective couplings to the left and right lead, ϕ_L and ϕ_R label the phases of the corresponding superconducting order parameter. The BCS gap Δ is assumed to be equal in both superconductors. In the model, defined by Eq. (1), the local Coulomb repulsion U is set to infinity.

the effective couplings $\Gamma_a = \pi N_0 V_a^2$ and $\Gamma = \Gamma_L + \Gamma_R$, where N_0 is the density of states at the Fermi energy in the normal conducting state.

The BCS part of the Hamiltonian can be easily solved. The normal and the anomalous local advanced/retarded conduction electron Green's functions are defined as $G_a^{A/R}(t) = \pm \sum_{\mathbf{k}} i\theta(\mp t) \langle \{c_{\mathbf{k}\sigma a}(t), c_{\mathbf{k}\sigma a}^\dagger(0)\} \rangle$ and $F_a^{A/R}(t) = \pm \sum_{\mathbf{k}} i\theta(\mp t) \langle \{c_{\mathbf{k}\uparrow a}(t), c_{-\mathbf{k}\downarrow a}(0)\} \rangle$, respectively. The gap equations defining the order parameter Δ_a in the two superconductors are given by $\Delta_a = V_{BCS} \sum_{\mathbf{k}} \langle c_{-\mathbf{k}\downarrow a} c_{\mathbf{k}\uparrow a} \rangle$. In the subsequent consideration the amplitude of Δ_a is assumed to be equal on both sides, i.e.

$$\Delta_a = |\Delta| e^{i\phi_a}. \quad (3)$$

For the local conduction electron density of states per spin and the corresponding anomalous contribution one obtains,

$$\rho_a(\epsilon) = \frac{G_a^A(\epsilon) - G_a^R(\epsilon)}{2\pi i N_0} = +\text{Re} \frac{|\epsilon|}{\sqrt{\epsilon^2 - |\Delta_a|^2}}, \quad (4a)$$

$$g_a(\epsilon) = \frac{F_a^A(\epsilon) - F_a^R(\epsilon)}{2\pi i N_0} = -\text{Re} \frac{\text{sign}(\epsilon)\Delta_a}{\sqrt{\epsilon^2 - |\Delta_a|^2}}, \quad (4b)$$

where both spectral functions have been normalized to N_0 .

For the greater part of this paper the Kondo dynamics of the quantum dot at finite temperatures will be described within a selfconsistent approach, where the local gauge symmetry on the dot is preserved by means of conserving approximations, derived from a Luttinger-Ward functional³¹. We will use a generalization of the well-known non-crossing approximation (NCA)^{32,33} for superconducting leads, the ‘‘superconducting NCA’’ (SNCA), to include retarded Cooper pair tunneling. The

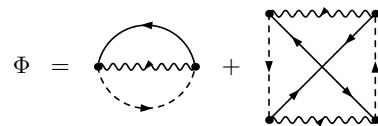


FIG. 2: Generating functional for the extension of the NCA to the broken-symmetry state (SNCA). The solid, wavy and dashed lines represent the conduction electron, slave boson and pseudofermion propagators, respectively.

Luttinger-Ward generating functional Φ for the SNCA is depicted in Fig. 2. The leading term of $O(\Gamma)$ in a selfconsistent expansion corresponds to the NCA (first diagram in Fig. 2). For normal conducting leads, the NCA is known to give a satisfactory, quantitative description of the spectral features in the case of infinite U ,^{34,35,36,37,38} in the absence of magnetic field,^{39,40} and for temperatures down to $T \approx 0.1 T_K$.³⁷ However, in the case of superconducting leads the NCA completely neglects Andreev scattering contributions (Cooper pair tunneling through the dot), which is crucial for the Josephson current and which will also induce significant renormalizations of the normal quasiparticle current, as seen below. Therefore, the NCA is extended to include the next-to-leading term of order $O(\Gamma^2)$ (second diagram in Fig. 2), which contains two anomalous lead Green's functions, constituting the SNCA.⁴¹ Similar, but simplified methods, employing an elastic scattering approximation, have also been used by Bickers and Zwicky⁴² and by Borkowski and Hirschfeld⁴³. A detailed discussion of the SNCA is deferred to Appendix A. It will be seen that the SNCA describes, to leading selfconsistent order, the coherent transmission of Cooper pairs via the formation of *retarded* Cooper pairs on the dot even though the existence of *equal-time* Cooper pairs on the dot is prohibited by the local Coulomb repulsion. Superconducting Kondo dot junctions have recently been considered also within a mean field approach to the dot dynamics,^{44,45} which tends to overestimate the Cooper pair correlations on the dot due to the assumption of static rather than retarded pairs on the dot.

From the generating functional in Fig. 2 a set of coupled integral equations for the pseudoparticle selfenergies can be derived as well as an expression for the local spectral function of the quantum dot and its corresponding anomalous part. These equations are solved numerically. The explicit expressions are discussed in Appendix A.

To calculate the Josephson current we use the formula first presented by Clerk and Ambegaokar¹⁸

$$I_s(\phi) = \frac{2e}{h} \frac{\Gamma}{\pi N_0} \sin \phi \int d\omega f(\omega) \times \text{Im} \left[\bar{\mathcal{F}}_d^{R\dagger}(\omega) \bar{F}^R(\omega) \right], \quad (5)$$

which is rederived in Appendix B. The quantities in this current relation are defined as follows: $\phi = \phi_L - \phi_R$ de-

notes the phase difference between left and right lead, $f(\omega)$ is the Fermi function and, for convenience, we extracted the explicit phase dependence from the off-diagonal Green's functions,

$$\begin{aligned}\mathcal{F}_d^R(\omega) &= \cos\left(\frac{\phi}{2}\right)\bar{\mathcal{F}}_d^R(\omega) \\ F_a^R(\omega) &= e^{i\phi_a}\bar{F}^R(\omega),\end{aligned}$$

where $\mathcal{F}_d^{R\dagger}(\omega)$ and $F_a^R(\omega)$ are the anomalous parts of the Green's function of the impurity d -level and of the conduction-electron Green's function in lead a , respectively (cf. Appendix B).

The zero bias conductance $G = dI/dV|_{V=0}$ is calculated from the quasiparticle current in the limit of small bias⁴⁶,

$$G = -2\frac{e^2}{h}\Gamma \int d\omega \frac{\partial f(\omega)}{\partial \omega} \rho(\omega) \text{Im}\mathcal{G}_d^A(\omega), \quad (6)$$

with $\mathcal{G}_d^A(\omega)$ the normal part of the impurity Green's function. As we consider a symmetric coupling to the two leads with equal spectral densities ($\Gamma_L = \Gamma_R \equiv \pi N_0 V_{L,R}^2$, $\Gamma \equiv \Gamma_L + \Gamma_R = 2\Gamma_{L,R}$, and $\rho_L(\omega) = \rho_R(\omega) \equiv \rho(\omega)$), all contributions with anomalous as well as with Keldysh Green's functions vanish in Eq. (6).

III. SUPERCURRENT

We now investigate the current-phase relation $I_s(\phi)$ in the parameter space which is controlled by temperature T and coupling strength T_K/Δ . This analysis focuses naturally on a calculation at finite T , for which regime the NCA yields quantitatively well controlled results³⁷ in the absence of magnetic field, and so is expected to do its superconducting extension, the SNCA. We will compare the $T \rightarrow 0$ extrapolation of these calculations with our perturbative renormalization group (RG) analysis of the same model at $T = 0$ as well as with exact numerical renormalization group (NRG) calculations by Choi *et al.*²⁷ at $T = 0$ for the symmetrical Anderson model.

It has been elaborated by Clerk and Ambegaokar¹⁸ that strong and weak coupling regimes are to be distinguished by the position of the subgap resonance: the resonance moves through the Fermi energy from below when the coupling is increased, a behavior to be associated with a transition from a π - to a 0-junction type. In fact, we confirm this behavior in Figs. 3 and 4. However, the resonance is wider than observed by Clerk and Ambegaokar: For strong coupling $T_K/\Delta > 1$, the subgap resonance as well as the features at the gap edges in the d -electron spectrum are of the order of $T_K > \Delta$, as Cooper pairs are broken in order to screen the impurity spin in this regime. The gap edges are less pronounced (see Fig. 3, lower panel), and a Fano-like interference between the continuum states and the subgap mode is evident.

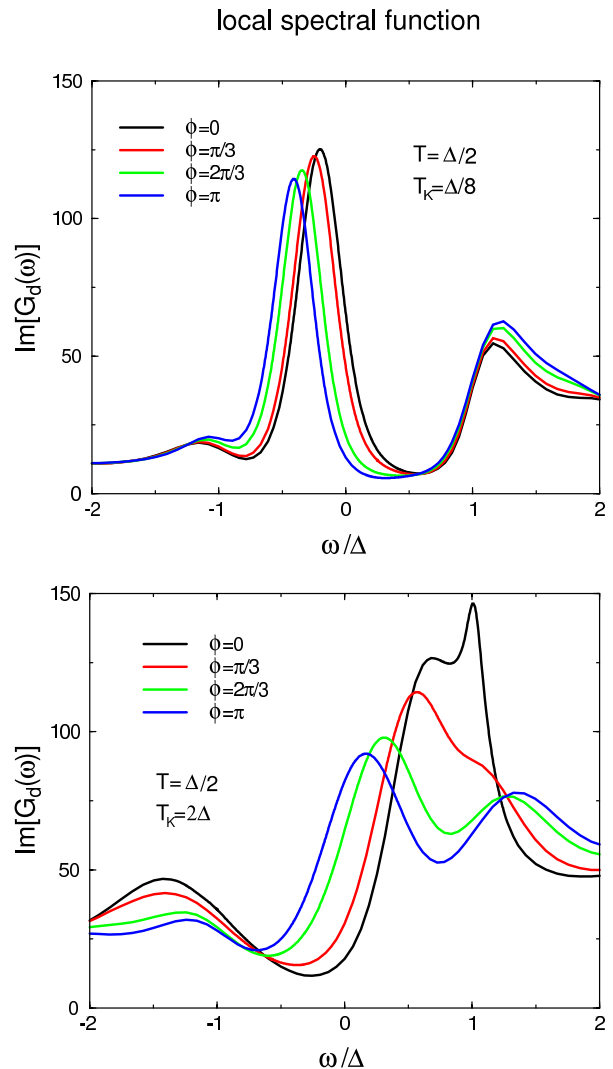


FIG. 3: The spectral function of the impurity d -level for weak coupling (upper panel, $T_K/\Delta = 0.125$) and strong coupling (lower panel, $T_K/\Delta = 2.0$). The leads are in the superconducting state at $T = 0.5\Delta$. The spectral functions are sensitive to the phase difference $\phi = \phi_L - \phi_R$ between left and right lead.

The current-phase relation traverses three scenarios or transitions, as the coupling parameter T_K/Δ is raised from weak to strong coupling (left column of Fig. 4). These scenarios are related to the fact that the Josephson current states of a superconducting junction are equilibrium states and are thus determined by the minima of the free energy. One may identify a succession of four current-carrying equilibrium states: 0-junction: single global minimum for $\phi = 0$; $0'$ -junction: global minimum for $\phi = 0$ and local minimum for $\phi = \pi$; π' -junction: local minimum for $\phi = 0$ and global minimum for $\phi = \pi$; π -junction: single global minimum for $\phi = \pi$. The succession of the corresponding transitions has been discussed in the literature^{47,48}.

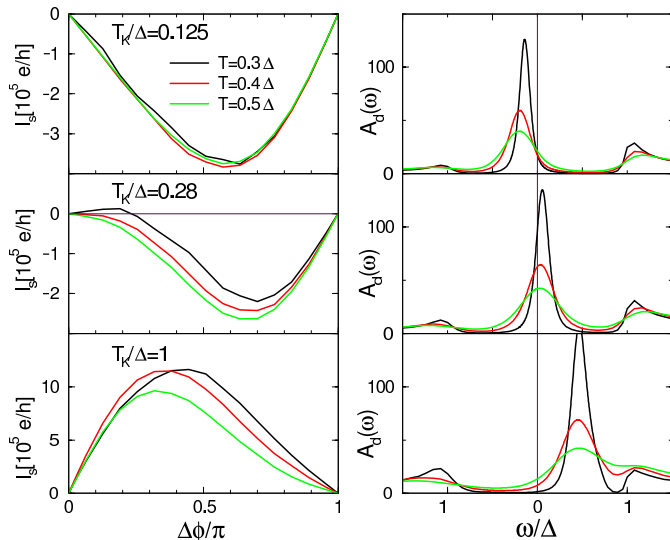


FIG. 4: Phase dependence of the Josephson current for weak, intermediate and strong coupling values of T_K/Δ (left column of panels). In the right panel, the spectral function of the impurity d -level is presented for each coupling strength and temperature.

1. *Weak coupling.* In the case $T_K/\Delta = 1/8$ all three curves $I_s(\phi)$ correspond to temperatures above T_K . The curves are nearly identical within numerical resolution. We observe a π -junction behavior where the first harmonic, $-\sin \phi$, dominates. In SNCA we cannot approach the low temperature limit where T is well below T_K . The latter has been investigated by Choi *et al.*²⁷ who indeed find a sinusoidal behavior for the zero temperature limit in the weak coupling regime.
2. *Intermediate coupling.* Here, higher harmonics become important (as in the second row of Fig. 4 for $T_K/\Delta = 0.28$). The derivative of the current at $\phi = 0$ changes sign with the temperature somewhere close to $T = 0.4\Delta$ (middle left panel), which corresponds approximately to temperature and coupling where the spectral function crosses the Fermi energy. Choi *et al.*²⁷ observe a discontinuous behavior in the current-phase relation for the intermediate coupling regime at zero temperature however this discontinuity is smoothed for finite temperature⁴⁹. The distinction between the $\pi - \pi'$, the $\pi' - 0'$ and the $0' - 0$ transitions, which classify the appearance and vanishing of the two minima of the free energy as mentioned above, is made by the characteristics of the current-phase relation: The sign reversal of the slope of $I_s(\phi)$ at vanishing ϕ in the intermediate coupling regime signifies the $\pi' - \pi$ transition.
3. *Strong coupling.* The lower left panel in Fig. 4

shows the current-phase relation for $\Delta/T_K = 1$. For this value of the coupling we are already in the strong coupling regime in the sense that the sub-gap resonance is clearly above the Fermi energy and the supercurrent is positive in the considered phase interval (0-junction behavior). The temperature of all curves is below T_K . The curve is more sinusoidal for the lowest temperature whereas it develops a flatter region for ϕ close to π for the higher temperatures. This is a precursor to the $0 - \pi$ transition and we will see below that the π -junction behavior may be recovered for higher temperature if T_K/Δ is not too large.

The phase diagram is now derived from the analysis of the extrema in the free energy: (i) the $\pi - \pi'$ transition takes place when the maximum at phase $\phi = 0$ turns into a local minimum of the free energy which is equivalent to the sign change of the slope of the current-phase relation for vanishing ϕ (circles in Fig. 5); (ii) the $\pi' - 0'$ transition refers to the point in the $(T, T_K/\Delta)$ -parameter space where the global minimum of the free energy switches from $\phi = \pi$ to $\phi = 0$ (triangles in Fig. 5); (iii) finally, the $0' - 0$ transition corresponds to the conversion of the local minimum at phase $\phi = \pi$ into a maximum, that is, the slope of $I_s(\phi)$ changes sign for phase π (squares in Fig. 5).

The symmetrical BCS-Anderson model has also been investigated by Siano and Egger⁴⁸ using the quantum Monte Carlo technique. However, Choi *et al.* point out that Ref. 48 does not consider the true low temperature limit and that the scales, such as the Kondo temperature, differ exponentially from the conventional definitions.^{49,50}

The zero temperature limit cannot be reached within the SNCA scheme. For this purpose we have performed a perturbative RG analysis, analogous to the poor man's scaling approach for the normal state⁵¹. In the one-loop evaluation, the vertex from the impurity coupling term

$$H_{\text{Kondo}} = \frac{J_K}{4} \sum_{\substack{\sigma\sigma' \\ \alpha\alpha'}} \sum_{\mathbf{k}\mathbf{k}'} f_{\alpha}^{\dagger} \vec{\tau}_{\alpha\alpha'} f_{\alpha'} c_{\mathbf{k}\sigma}^{\dagger} \vec{\sigma}_{\sigma\sigma'} c_{\mathbf{k}\sigma'} \quad (7)$$

generates particle-particle and particle-hole loops of conduction and pseudofermion Green's functions. Here J_K is the Kondo coupling ($J_K = V^2/|\epsilon_d|$ for $U \rightarrow \infty$) and τ^i (σ^i) are the Pauli matrices in the impurity spin space (conduction electron spin space).

While these diagrams renormalize the Kondo coupling in the normal state, one-loop contributions with an anomalous conduction electron propagator are to be included for the superconducting state. Although the corresponding vertex is missing in the bare Hamiltonian, the RG flow will generate the coupling which is of the form

$$H_g = \sum_{\substack{\sigma\sigma' \\ \alpha\alpha'}} \sum_{\mathbf{k}} \frac{g_{ij}}{4} f_{\alpha}^{\dagger} \tau_{\alpha\alpha'}^i f_{\alpha'} c_{\mathbf{k}\sigma}^{\dagger} \sigma_{\sigma\sigma'}^j c_{-\mathbf{k}\sigma'} \quad (8)$$

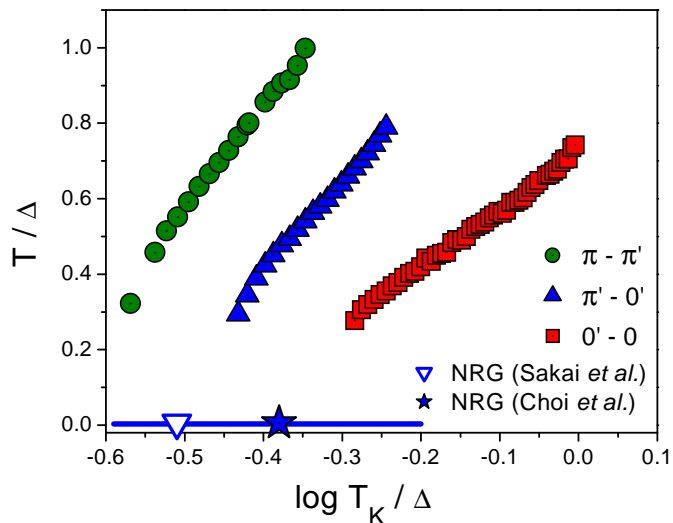


FIG. 5: Phase diagram for the $0-\pi$ transitions. As discussed in the text, the lower right area corresponds to the 0 -phase and the upper left area to the π -phase. The SNCA data points refer to the $\pi-\pi'$ transition (circles), the $\pi'-0'$ transition (triangles), and the $0'-0$ transition (squares). As seen from these curves, the respective transition points as a function of T scale roughly with $\log T_K$. The open inverse triangle presents the transition point from a spin doublet to a singlet state of a Kondo impurity in a bulk superconductor within the NRG evaluation of Satori *et al.*⁵³. The star on the horizontal axis is approximately the transition point in the NRG analysis for the symmetric Anderson model of the quantum dot contact (Choi *et al.*²⁷). The fat line at the horizontal axis is the regime where the perturbative RG analysis suggests the $\pi'-0'$ transition at zero temperature.

This coupling term will have the effect of cutting the RG flow for small T_K/Δ , that is, in the perturbative regime. Only the coupling term with g_{02} will be renormalized under the RG flow, a consequence of spin conservation and the symmetry of the order parameter.

With the initial conditions of isotropic spin coupling and zero potential scattering term, the following RG equations are obtained:⁵²

$$\frac{dJ}{d \ln D} = -\text{Re} \left[\frac{D}{\sqrt{D^2 - \Delta^2}} \right] \left(J^2 - 2 \frac{\Delta}{D} Jg \right) \quad (9a)$$

$$\frac{dg}{d \ln D} = -\text{Re} \left[\frac{D}{\sqrt{D^2 - \Delta^2}} \right] \left(2 \frac{\Delta}{D} g^2 + \frac{3}{2} \frac{\Delta}{D} J^2 \right) \quad (9b)$$

where D is half the band width and the dimensionless couplings are defined as:

$$J = N_0 J_K \quad \text{and} \quad g = -i N_0 g_{02}. \quad (10)$$

Here g denotes the local coupling of pair fluctuations to the impurity with the initial condition $g(D_0) = 0$ for the bare band cut-off D_0 . For $\Delta \rightarrow 0$ one recovers the standard poor man's scaling result.

For weak coupling ($T_K/\Delta \lesssim 0.25$) the effective bandwidth D approaches Δ before J or g diverge; the square root in the scaling Eqs. (9) then vanishes and cuts off the RG flow. The scaling trajectories in the $J-g$ plane flow towards a line of such fixed points. The ground state is an unscreened spin. The strong coupling regime is only accessible within a non-perturbative analysis but the tendency of the trajectories to flow away from the fixed point line towards a strong coupling fixed point with $J = \infty$ is already observed in the present one-loop evaluation. The strong coupling fixed point is approached for a bare coupling strength above a minimal T_K/Δ somewhere in between 0.25 and 0.65.

The solid fat line at the horizontal axis in Fig. 5 indicates the range where this quantum phase transition ($\pi'-0'$ transition) is supposed to take place. The range is certainly too wide in order to estimate the low temperature extrapolation of the intermediate temperature data. However the transition range is consistent with the SCNA results. This does not apply for the extrapolated transition value of Clerk and Ambegaokar¹⁸ which is already at positive values of $\log(T_K/\Delta)$. We do not well understand the discrepancy to the result of Clerk and Ambegaokar; it may be related to the way in which the zero temperature limit was approached in Ref. 18. However the NRG result of Choi *et al.*²⁷ (with transition at $T_K/\Delta \simeq 0.42$, star in Fig. 5) for the particle-hole symmetric model is within our estimate from the 1-loop RG. Yet this comparison should be taken with caution as the

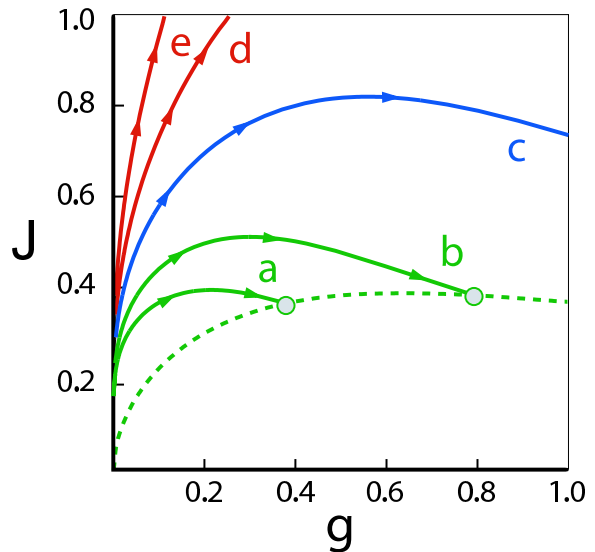


FIG. 6: Scaling trajectories for various bare coupling values: (a) $T_K/\Delta = 0.1$, (b) $T_K/\Delta = 0.2$, (c) $T_K/\Delta = 0.5$, (d) $T_K/\Delta = 1$, and (e) $T_K/\Delta = 2$. The open circles represent fixed points, the dashed line is the fixed point line. The last fixed point in the perturbative regime is found for $T_K/\Delta \simeq 0.25$. For $T_K/\Delta \simeq 0.65$ no downturn of the trajectory is observed. In the limit $T_K/\Delta \rightarrow \infty$ the trajectory follows the J -axis towards strong coupling.

particle-hole symmetric Anderson model also allows for local equal-time pair correlations (of the f -particles) and has no potential scattering term, both in contrast to the infinite- U case. The potential scattering term present in the asymmetric model induces a characteristic shift of the Kondo resonance relative to the Fermi energy,²¹ and thus is expected to influence the 0 - π transition as well. The transition from the spin doublet to a singlet state of a Kondo impurity in a bulk superconductor was calculated within NRG by Satori *et al.*⁵³ They found $T_K/\Delta \simeq 0.3$ which is presented by the open triangle in Fig. 5. This NRG result is within the range of our 1-loop RG estimate and appears to be in agreement with the finite-temperature SNCA data.

It should be obvious from the phase diagram that the transition is not only achieved by a change of the coupling parameter T_K/Δ (through, e.g., gating the quantum dot) but also by a temperature variation, provided that the (fixed) coupling is in an intermediate range.

IV. ZERO BIAS CONDUCTANCE

The Josephson current directly probes the phase-sensitive anomalous Green's functions (see Eq. (5)). The conductance, however, is related to the quasiparticle current and it is expressed through the imaginary parts of the diagonal Green's functions: it has a finite, measurable value if the derivative of the Fermi function is not exponentially small and if the bulk density of states (i.e., $\text{Im}G^A(\omega)$) and the impurity spectral function ($\text{Im}\mathcal{G}_d^A(\omega)$) are both finite in the same frequency interval (see Eq. (6)). This implies that the conductance vanishes exponentially for the zero temperature limit as we restrict our considerations to s -wave superconductors.

The question arises if this conductance of the quantum dot exhibits a signature of the 0 - π transition at all. The solution to this elementary question is not straightforward since the conductance does not directly expose the phase dependence of the superconducting states in the leads. However, as the position of the subgap resonance moves from below through the Fermi energy with increasing coupling, the ground state transits into a singlet state through the Kondo screening of the impurity spin. The enhanced screening, which is possible for strong coupling, not only modifies the subgap resonance but also the continuum through increased pair breaking in this regime (cf. Fig. 3). Correspondingly, one may expect a feature in the temperature-dependent or coupling- (T_K/Δ -) dependent conductance which signifies the transition. This can be expected only if the temperature is not too small (with respect to Δ) so that $\partial f/\partial\omega$ in Eq. (6) is still sizable for frequencies with finite $\rho(\omega)$.

Consequently, the conductance G , Eq. (6), represents an integral with respect to the quasiparticle energy ω over an interval of the order of T . In order to exhibit characteristic features of the local spectral density in the finite- T conductance it is, therefore, suggestive

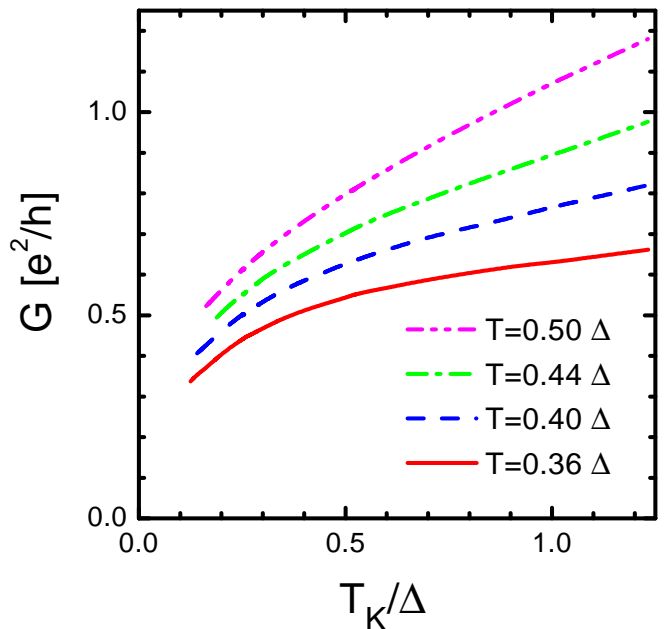


FIG. 7: Zero bias conductance G as a function of coupling strength T_K/Δ for fixed temperature.

to analyse the temperature derivative dG/dT . Equivalently, one may consider the coupling parameter derivative, $dG/d(T_K/\Delta)$, because G is expected to be a universal function in terms of T/T_K for fixed Δ . At finite T and fixed Δ , both dG/dT and $dG/d(T_K/\Delta)$ may be expected, in a rough first estimate, to be essentially proportional to $\text{Im}\mathcal{G}_d^A(\omega = T)$ and $\text{Im}\mathcal{G}_d^A(\omega = T_K)$, respectively, disregarding the energy dependence of the quasiparticle density of states in the leads — a more refined analysis certainly has to take the detailed frequency structure of the integrand into account. Hence, in the weak coupling regime ($\ln(\Delta/T_K) \gg 1$, $\ln(T/T_K) \gg 1$) we expect

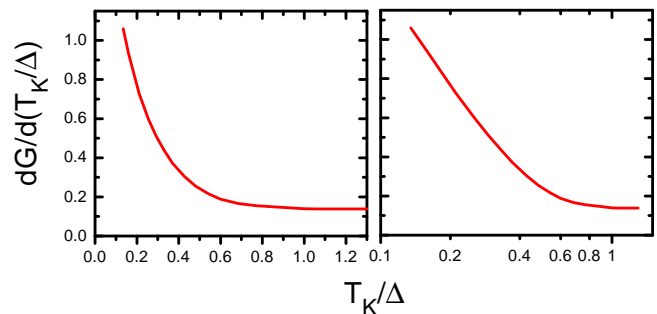


FIG. 8: Derivative of the zero bias conductance, $G(T_K/\Delta)$, with respect to the coupling parameter at $T/\Delta = 0.36$. Left frame: linear scales; the π' - $0'$ transition is at approximately $T_K/\Delta \simeq 0.4$, for strong coupling $dG/d(T_K/\Delta)$ is constant. Right frame: coupling scale is in logarithmic presentation; for weak coupling $dG/d(T_K/\Delta)$ diverges logarithmically.

approximately that $dG/d(T_K/\Delta) \propto -\ln(T_K/\Delta)$, while in the strong coupling region ($T_K/\Delta \gtrsim 1$, $T/\Delta < 1$), $dG/d(T_K/\Delta)$ should be approximately T and T_K independent. This expected linear behavior of G for large coupling strength, where Kondo screening is dominant, is associated with the formation of the Kondo resonance as it collects spectral weight and saturates at energies below T_K .

For the numerical evaluation we focus on the lowest temperature in Fig. 7 ($T/\Delta = 0.36$, continuous line). The conductance displays a constant slope in the 0-phase ($T_K/\Delta \gtrsim 0.4$), whereas in the π -phase ($T_K/\Delta \lesssim 0.4$) the slope of G tends to diverge for $T_K \rightarrow 0$. This crossover is even more apparent from the derivate of the conductance with respect to T_K/Δ (see the left panel of Fig. 8 and the discussion above). Clear logarithmic behavior of the slope is observed in the π -phase, where the numerical SNCA results are especially controlled (see right panel of Fig. 8). The crossover between constant slope and logarithmic behavior is found to be at a coupling strength which corresponds to the 0- π transition. In fact, for $T/\Delta = 0.36$, the π' -0' transition is at approximately $T_K/\Delta \simeq 0.4$.

Finally, we explore the temperature dependence of the quantum dot conductance. In Fig. 9 we present the SNCA results for the zero bias conductance G versus temperature T at fixed values of T_K/Δ . The exponential regime for very low temperatures is outside the range where the SNCA is reliable. For the low temperature limit $\partial f/\partial\omega$ is exponentially small for $\omega > |\Delta|$ and should control the temperature dependence of the conductance. However, with our data we are still in the regime with a wide derivative of the Fermi function and a negative curvature of the $G(T)$ lines. Fig. 9 suggests to assign a constant slope to the conductance in this intermediate

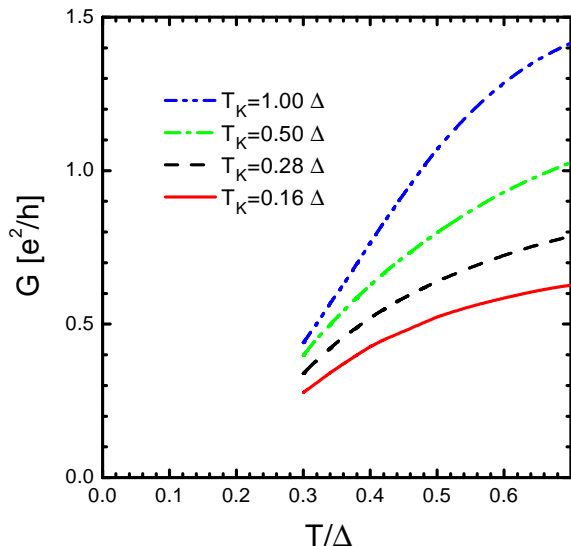


FIG. 9: Zero bias conductance G as a function of temperature T/Δ for fixed coupling strengths T_K/Δ .

temperature range for the strong coupling regime. Such a linear behavior in $G(T)$, Eq. (6), is generated by an approximate compensation of the sharp spectral structures in $\rho(\omega)$ and in $\text{Im}\mathcal{G}_d^A(\omega)$ at the gap edge. The integration over the derivative of the Fermi function yields the linear dependence for the intermediate temperature range — although the non-leading contributions to the frequency dependence above the gap edge may alter the temperature dependence. The linear temperature behavior is consistent with the linear T_K dependence of G which was discussed before. For the weak coupling regime one should expect a $\ln T$ dependence of dG/dT . The temperature range for the lowest curve in Fig. 9 (with $T_K/\Delta = 0.16$) is too narrow to decide about a logarithmic divergence of dG/dT but the few data points are consistent with this assumption.

V. CONCLUSION

In conclusion, we have calculated the Josephson current as well as the linear response quasiparticle conductance for quantum dots in the Kondo regime with superconducting leads. For finite temperatures, we have used a superconducting extension of the non-crossing approximation (SNCA), while for $T = 0$ the behavior was analyzed using a perturbative renormalization group treatment. In this way we mapped out the phase diagram of the 0- π transition of the Josephson current in the parameter space of temperature and Kondo coupling constant for the first time in a systematical way. We stress that for temperatures not too far below T_K the SNCA is expected to produce reliable, semiquantitative results. The $T \rightarrow 0$ extrapolation of our results agrees well with an NRG treatment of the problem at $T = 0$,²⁷ considering that the latter was done for the finite- U symmetric Anderson model which, on one hand, allows for equal-time Cooper pair formation on the dot, and, on the other hand, does not have a potential scattering term — both in contrast to our asymmetric, infinite- U model. Considering finite T will be essential for the analysis of experiments (see below).

Our results confirm that the Josephson current undergoes a succession of three transitions, 0 - 0', 0' - π' , π' - π , separating four different Josephson equilibrium states, as the Kondo temperature T_K is reduced below the superconducting gap energy Δ , or, alternatively, as the temperature T is raised above T_K . In going from a 0-type to a π -type junction, the four types of Josephson junctions are related to the successive development of the minima of the free energy^{47,48}. By explicit calculations we could relate these phases to the characteristic phase dependence of the Josephson current as well as to the position of the Kondo-like subgap resonance above or below the Fermi energy. Moreover, we have also identified the signature of the 0- π transition in the quasiparticle linear response conductance G . Since the latter vanishes exponentially for $T \rightarrow 0$, a treatment at finite T was essential

here. From our results, the 0-junction regime appears to be characterized by a constant slope of the conductance as a function of T_K/Δ , while in the π -junction regime the slope diverges logarithmically. Note that at finite T the 0- π transitions are continuous crossovers because of the finite width of the subgap resonance and develop a discontinuous jump only for $T \rightarrow 0$ with vanishing width of the subgap resonance.²⁷ These relations may be relevant for identifying and analyzing the different phases in experiments like quantum dots, carbon nanotubes or other Kondo molecules coupled to superconducting leads. Gated devices are supposed to control the level position in the quantum dot and, correspondingly, the Kondo scale.

Acknowledgments

The authors are grateful to Peter Wölfle for discussions and support. G.S. and J.K. acknowledge discussions with Stefan Kirchner. This work is supported by BMBF 13N6918A (T.K., G.S.), DAAD D/03/36760 (T.K.), NSF-INT-0340536 (Y.S.B.), RFBR grant No. 05-02-17175 (Y.S.B.) and by the Deutsche Forschungsgemeinschaft through CFN (G.S.), SFB 484 (T.K., G.S.) and through grant No. KR1726/1 (J.K.).

APPENDIX A: SUPERCONDUCTING NCA (SNCA)

In this appendix, we give a detailed derivation and discussion of the formulae for the selfenergies, the auxiliary particle propagators and the local electron Green's function within the SNCA. The same approximation has been used by Clerk and Ambegaokar in Refs. 18,41.

The BCS-Anderson Hamiltonian Eq. (1) obeys a local $U(1)$ gauge symmetry with respect to simultaneous, time dependent transformations of the auxiliary particle fields,

$$f_\sigma \rightarrow e^{i\varphi(t)} f_\sigma, \quad b \rightarrow e^{i\varphi(t)} b, \quad \lambda \rightarrow \lambda - \frac{\partial\varphi}{\partial t}, \quad (\text{A1})$$

which is intimately related to the conservation of the local charge Q , and which, due to Elitzur's theorem, cannot be broken.⁵⁴ The local gauge symmetry is implemented in the standard way,³¹ where a conserving, selfconsistent approximation is generated from a Luttinger-Ward functional via functional derivative with respect to the renormalized pseudoparticle propagators as well as the lead Green's functions.^{55,56} In addition, the constraint $Q = 1$ is enforced in any expectation value of a *physical* operator acting on the impurity state (more precisely: any operator which annihilates the $|Q = 0\rangle$ state) by taking the limit $\lambda \rightarrow \infty$; e.g. for the physical d -electron Green's function,^{30,37}

$$\mathcal{G}_{d\sigma}(t) = -i \lim_{\lambda \rightarrow \infty} \frac{\langle d_\sigma(t) d_\sigma^\dagger(0) e^{-\beta H - \beta \lambda(Q-1)} \rangle}{\langle Q e^{-\beta H - \beta \lambda(Q-1)} \rangle}, \quad (\text{A2})$$

FIG. 10: Pseudofermion selfenergy $\Sigma(i\omega)$ and slave boson selfenergy $\Pi(i\nu)$

with $\langle \dots \rangle$ the time-ordered, grand canonical expectation value and $\beta = 1/T$.

Implications of the projection $Q = 1$. The constraint crucially influences the auxiliary particle dynamics and, in particular, prohibits any anomalous contributions to the auxiliary particle propagators, even in the case of superconducting leads. Consider, for example, the Nambu pseudofermion propagator,

$$\mathbf{F}_\sigma(\omega) = -i\Theta(t) \left\langle \left\{ \begin{pmatrix} f_\sigma \\ f_{-\sigma}^\dagger \end{pmatrix}, \begin{pmatrix} f_\sigma^\dagger \\ f_{-\sigma} \end{pmatrix} \right\} \right\rangle_{\omega} \quad (\text{A3})$$

$$= \begin{pmatrix} \omega - \epsilon_d - \lambda - \Sigma_\sigma(\omega) & -\Sigma_\sigma^{anom}(\omega) \\ -\Sigma_\sigma^{anom}(-\omega) & \omega + \epsilon_d + \lambda + \Sigma_{-\sigma}(-\omega) \end{pmatrix}^{-1},$$

where Σ_σ is the normal selfenergy, and the anomalous selfenergy Σ_σ^{anom} is assumed non-zero for the moment. Using the gauge $(\omega - \lambda) \rightarrow \omega$, performing the matrix inversion in Eq. (A3), and then taking the limit $\lambda \rightarrow \infty$ proves that all but the (11) element of the pseudofermion propagator, $F_\sigma(\omega) \equiv [\mathbf{F}_\sigma(\omega)]_{11}$, vanish. An analogous proof holds for the slave boson propagator. As a result, the (retarded) pseudofermion and slave boson propagators $F^R(\omega)$, $B^R(\omega)$, respectively, have only normal contributions,

$$F^R(\omega) = (\omega - \epsilon_d - \lambda - \Sigma^R(\omega))^{-1} \quad (\text{A4a})$$

$$B^R(\omega) = (\omega - \lambda - \Pi^R(\omega))^{-1}, \quad (\text{A4b})$$

where $\Sigma^R(\omega)$, $\Pi^R(\omega)$ are the pseudofermion and slave boson selfenergies, respectively, and the spin index has been suppressed in the absence of a magnetic field.

The evaluation of the Matsubara sum over a pseudoparticle frequency shows that each closed pseudoparticle loop carries a fugacity factor $e^{-\beta\lambda}$. Hence, upon the projection $\lambda \rightarrow \infty$ the Luttinger-Ward generating functional is comprised of diagrams which contain exactly one closed pseudoparticle loop: Its vanishing fugacity factor is cancelled by the corresponding factor $e^{-\beta\lambda}$ of the term $\langle Q e^{-\beta H - \beta \lambda(Q-1)} \rangle$ in the denominator of any physical expectation value [see Eq. (A2)].

Definition of the SNCA. To define a conserving approximation that describes coherent Cooper pair transmission through a Kondo quantum dot, the generating functional shown diagrammatically in Fig. 2 has been chosen. The first diagram of Fig. 2 represents the conventional non-crossing approximation and describes normal quasiparticle transmission. The second diagram of Fig. 2 contains

two crossing anomalous superconducting Green's functions in the leads. It is the simplest (i.e. lowest order in the hybridization V_a) contribution to incorporate coherent Cooper pair tunneling in the Luttinger-Ward functional. Therefore, the corresponding approximation has been termed "superconducting non-crossing approximation" (SNCA). The resulting auxiliary particle selfenergies Σ , Π , are shown in Fig. 10 and read,

$$\begin{aligned} \Sigma^R(\omega) &= \sum_a \frac{\Gamma_a}{\pi} \int d\epsilon f(\epsilon) \rho_a(-\epsilon) B^R(\epsilon) \\ &\quad - \sum_{aa'} \frac{\Gamma_a \Gamma_{a'}}{\pi^2} \int d\epsilon f(\epsilon) g_a^*(\epsilon) \int d\epsilon' f(\epsilon') g_{a'}(\epsilon') \\ &\quad \times B^R(\omega + \epsilon) B^R(\omega + \epsilon') F^R(\omega + \epsilon + \epsilon'), \quad (\text{A5a}) \end{aligned}$$

$$\begin{aligned} \Pi^R(\omega) &= \sum_a \frac{N \Gamma_a}{\pi} \int d\epsilon f(\epsilon) \rho_a(\epsilon) F^R(\epsilon) \\ &\quad + \sum_{a'} \frac{N \Gamma_a \Gamma_{a'}}{\pi^2} \int d\epsilon f(\epsilon) g_a(\epsilon) \int d\epsilon' f(\epsilon') g_{a'}^*(\epsilon') \\ &\quad \times F^R(\omega + \epsilon) F^R(\omega + \epsilon') B^R(\omega + \epsilon + \epsilon'), \quad (\text{A5b}) \end{aligned}$$

where $f(\epsilon)$ is the Fermi distribution function and $N = 2$ is the spin degeneracy. As seen from Fig. 10, the SNCA incorporates exactly two coherent Andreev transmission terms, one where a pseudofermion disappears from the dot and forms a Cooper pair in the superconducting lead, leaving an additional, virtual pseudofermion hole with opposite spin behind, and one describing the inverse process. Incoherent, sequential Andreev processes are included in the propagators to infinite order via self-consistency. The set of equations (A5) can be further simplified in extracting the explicit phase-dependence of the conduction electron functions, i.e.

$$\begin{aligned} \sum_a \Gamma_a \rho_a(\epsilon) &= \Gamma \rho(\epsilon), \\ \sum_{aa'} \Gamma_a \Gamma_{a'} g_a(\epsilon) g_{a'}^*(\epsilon') &= \Gamma^2 \cos^2\left(\frac{\phi}{2}\right) |g(\epsilon)| |g(\epsilon')|. \end{aligned}$$

Here, we have defined the phase difference $\phi = \phi_L - \phi_R$ and, and assumed symmetrical superconductors in the leads, $|g_L(\epsilon)| = |g_R(\epsilon)| \equiv |g(\epsilon)|$, $\rho_L(\epsilon) = \rho_R(\epsilon) \equiv \rho(\epsilon)$. By means of these relations it is seen immediately that only the terms with anomalous conduction electron propagators contribute to the phase dependence of the selfenergies in Eqs. (A5).

The equations for the normal and for the anomalous, physical dot electron Green's function are derived analogously by functional derivative of the generating functional with respect to the corresponding lead electron

propagators. This yields (see Fig. 11),

$$\text{Im} \mathcal{G}_d^R(\omega) = - \int \frac{d\epsilon}{\pi} e^{-\beta\epsilon} \text{Im} F^R(\epsilon + \omega) \text{Im} B^R(\epsilon), \quad (\text{A6a})$$

$$\begin{aligned} \text{Im} \mathcal{F}_d^R(\omega) &= - \Gamma \cos\left(\frac{\phi}{2}\right) \int \frac{d\epsilon}{\pi} e^{-\beta\epsilon} \int \frac{d\epsilon'}{\pi} f(\epsilon') |g(\epsilon')| \\ &\quad \times \text{Im} [F^R(\epsilon + \omega) B^R(\epsilon + \epsilon' + \omega)] \\ &\quad \times \text{Im} [F^R(\epsilon + \epsilon') B^R(\epsilon)]. \quad (\text{A6b}) \end{aligned}$$

Without loss of generality we have set $\phi_L + \phi_R = 0$. Note that, although the local U(1) gauge symmetry on the dot prevents anomalous contributions to the auxiliary particle propagators, anomalous physical electron Green's functions on the dot do exist. Physically this means that temporally retarded Cooper pairs on the quantum dot are indeed induced by the proximity effect, even though the formation of equal-time Cooper pairs is completely suppressed by the local Coulomb repulsion.

Numerical evaluation of the SNCA. The Eqs. (A4) and (A5) form a closed set of non-linear integral equations for the auxiliary particle propagators which is solved numerically by iteration. The physical dot electron Green's functions, which determine the Josephson as well as the quasiparticle current (see Appendix B), are then computed using Eqs. (A6). Note, however, that the Boltzmann factors in Eqs. (A6) strongly diverge for negative frequencies. Although this divergence is compensated by the threshold behavior of the pseudoparticle propagators, a numerical evaluation necessitates a re-formulation in terms of a new set of functions, $\text{Im} \tilde{F}(\omega)$, $\text{Im} \tilde{B}(\omega)$. We define them via the relations

$$\begin{aligned} \text{Im} F^R(\omega) &= f(-\omega) \text{Im} \tilde{F}(\omega), \\ \text{Im} B^R(\omega) &= f(-\omega) \text{Im} \tilde{B}(\omega). \end{aligned}$$

Since the Boltzmann factors appear precisely in conjunction with the integrals along the branch cuts of the auxiliary particle Green's functions, it is possible to absorb all these exponentially diverging factors in $\text{Im} \tilde{F}(\omega)$, $\text{Im} \tilde{B}(\omega)$ by observing $e^{-\beta\omega} f(-\omega) = f(\omega)$. Details of this method as well as of the efficient treatment of the projection $\lambda \rightarrow \infty$ can be found in Ref. 37.

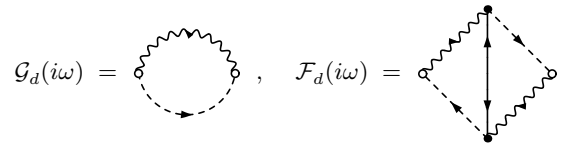


FIG. 11: Diagonal element $\mathcal{G}_d(i\omega)$ and off-diagonal element $\mathcal{F}_d(i\omega)$ of the impurity Green's function.



FIG. 12: Diagrams for $G_{\mathbf{k}\sigma a, \sigma}^<$; The double line represents the dot electron Green's function, the single line the conduction electron green's function. The left diagram contributes to the normal current, the second diagram contributes to the supercurrent, Eq. (B4)

APPENDIX B: JOSEPHSON CURRENT THROUGH AN INTERACTING REGION

A formula for the supercurrent through an interacting region is derived. We proceed along the line of references 18,46. The charge current through the system can be expressed by means of the time derivative of the electron numbers $N_{L/R}$ in the left and right lead, i.e.

$$I_{L/R} = \mp \langle \dot{N}_{L/R}(t) \rangle, \quad (\text{B1})$$

Note that the relation $I_L = I_R$ holds. The time derivative is calculated using the Heisenberg equation of motion, yielding the expression

$$I_a = \eta_a \frac{ie}{\hbar} \sum_{\mathbf{k}\sigma} V_a \left(\langle d_{\sigma'}^\dagger c_{\mathbf{k}\sigma, a} \rangle - \text{h.c.} \right) \quad (\text{B2})$$

with $\eta_{L/R} = \mp 1$. Using the definition for the lesser function $G_{\mathbf{k}\sigma a, \sigma'}^<(t, t') = i \langle d_{\sigma'}^\dagger(t') c_{\mathbf{k}\sigma, a}(t) \rangle$, I_a may be rewritten as

$$I_a = \eta_a \frac{2e}{\hbar} \sum_{\mathbf{k}\sigma} V_a \text{Re} \left[G_{\mathbf{k}\sigma a, \sigma}^<(0) \right]. \quad (\text{B3})$$

The diagrams contributing to $G_{\mathbf{k}\sigma a, \sigma}^<$ are shown in figure 12. In the following, the system is assumed to be in

equilibrium, i.e. $eV = 0$. In this limit the normal current vanishes, and charge is transferred through the system only via the supercurrent I_s , with

$$I_{s,a} = \eta_a \frac{2e}{\hbar} \sum_{\mathbf{k}\sigma} V_a^2 \int \frac{d\omega}{2\pi} \text{Re} \left[\mathcal{F}_d^{\dagger, A}(\omega) F_{\mathbf{k}a}^A(\omega) - \mathcal{F}_d^{\dagger, R}(\omega) F_{\mathbf{k}a}^R(\omega) \right]. \quad (\text{B4})$$

To derive the above equation we have used the relations $G(\omega) = G^<(\omega) - G^A(\omega)$ and $\bar{G}(\omega) = G^R(\omega) - G^<(\omega)$ for the time ordered and anti-time ordered Green's functions, respectively, and $G^<(\omega) = f(\omega) (G^A(\omega) - G^R(\omega))$ for the lesser functions. For convenience we extract the explicit phase dependence from the off-diagonal Green's functions,

$$\mathcal{F}_d^{R\dagger}(\omega) = \cos\left(\frac{\phi}{2}\right) \bar{\mathcal{F}}_d^{R\dagger}(\omega),$$

$$F_a^R(\omega) = e^{i\phi_a} \bar{F}^R(\omega),$$

where we have introduced the retarded, local conduction electron Green's function $F_a^R(\omega) = \sum_{\mathbf{k}} F_{\mathbf{k}a}^R(\omega)$. Moreover, without loss of generality we have set $\phi_L + \phi_R = 0$. Finally, using local charge conservation in the stationary case, $I_{s,L} = -I_{s,R} \equiv I_s$, we obtain the following formula for the Josephson current¹⁸

$$I_s = \frac{2e}{\hbar} \frac{\Gamma}{\pi N_0} \sin(\phi) \int d\omega f(\omega) \times \text{Im} \left[\bar{\mathcal{F}}_d^{R\dagger}(\omega) \bar{F}^R(\omega) \right], \quad (\text{B5})$$

with $\Gamma = \Gamma_L + \Gamma_R$.

* Electronic address: thilo.kopp@physik.uni-augsburg.de
¹ J. Appelbaum, Phys. Rev. Lett. **17**, 91 (1966).
² P.W. Anderson, Phys. Rev. Lett. **17**, 95 (1966).
³ L.I. Glazman and M.E. Raikh, JETP Lett. **47**, 452 (1988).
⁴ T.K. Ng and P.A. Lee, Phys. Rev. Lett. **61**, 1768 (1988).
⁵ I.L. Aleiner, P.W. Brouwer, and L.I. Glazman, Phys. Repts. **358**, 309 (2002).
⁶ H. Shiba and T. Soda, J. Phys. Soc. Japan **41**, 25 (1969).
⁷ L.I. Glazman, K.A. Matveev, JETP Lett. **49**, 659 (1989).
⁸ P. Schwab and R. Raimondi, Phys. Rev. B **59**, 1637 (1999).
⁹ J.C. Cuevas, A. Levy Yeyati, and A. Martin-Rodero, Phys. Rev. B **63**, 094515 (2001).
¹⁰ E. Scheer, P. Joyez, D. Esteve, C. Urbina, M.H. Devoret, Phys. Rev. Lett. **78**, 3535 (1997).
¹¹ E. Scheer, N. Agraït, J.C. Cuevas, A. Levy Yeyati, B. Ludoph, A. Martin-Rodero, G.R. Bollinger, J.M. van Ruitenbeek, C. Urbina, Nature **394**, 154 (1998).
¹² S. Sasaki, S. De Franceschi, J.M. Elzerman, W.G. van der Wiel, M. Eto, S. Tarucha, and L.P. Kouwenhoven, Nature **405**, 764 (2000).

¹³ J. Park, A.N. Pasupathy, J.I. Goldsmith, C. Chang, Y. Yaish, J.R. Petta, M. Rinkoski, J.P. Sethna, H.D. Abruna, P.L. McEuen, D. Ralph, Nature **417**, 722 (2002).
¹⁴ B. Babić and C. Schönenberger, Phys. Rev. Lett. **88**, 156801 (2002).
¹⁵ N. Agraït, A. Levy Eyati, and J.M. van Ruitenbeek, Phys. Rep. **377**, 81 (2003).
¹⁶ B. Babić, T. Kontos, and C. Schönenberger, Phys. Rev. B **70**, 235419 (2004).
¹⁷ P. Recher, E.V. Sukhorukov, and D. Loss, Phys. Rev. B **63**, 165314 (2001); P. Recher and D. Loss, Phys. Rev. B **65**, 165327 (2002); C. Bena, S. Vishveshwara, L. Balents, and M.P.A. Fisher, Phys. Rev. Lett. **89**, 037901 (2002).
¹⁸ A.A. Clerk and V. Ambegaokar, Phys. Rev. B **61**, 9109 (2000).
¹⁹ B.I. Spivak and S.A. Kivelson, Phys. Rev. B **43**, 3740 (1991).
²⁰ A.V. Rozhkov and D.P. Arovav, Phys. Rev. B **62**, 6687 (2000).

- ²¹ For a detailed analysis of the position of the Kondo resonance in the normal conducting state see, e.g. S. Kirchner, J. Kroha, and P. Wölfle, Phys. Rev. B **70**, 165102 (2004).
- ²² M. Fogelström, Phys. Rev. B **62**, 11812 (2000).
- ²³ Yu.S. Barash and I.V. Bobkova, Phys. Rev. B **65**, 144502 (2002).
- ²⁴ M. Andersson, J.C. Cuevas, and M. Fogelström, Physica C **367**, 117 (2002).
- ²⁵ N.M. Chtchelkatchev, W. Belzig, Yu.V. Nazarov, and C. Bruder, JETP Lett. **74**, 323 (2001).
- ²⁶ M. Pustilnik and L. Glazman, J. Phys.: Condens. Matter **16**, R513 (2004).
- ²⁷ M.-S. Choi, M. Lee, K. Kang, and W. Belzig, Phys. Rev. B **70**, 020502(R) (2004).
- ²⁸ M.R. Buitelaar, T. Nussbaum, and C. Schönberger, Phys. Rev. Lett. **89**, 256801 (2002).
- ²⁹ S. E. Barnes, J. Phys. F **6**, 1375 (1976); **7**, 2637 (1977).
- ³⁰ P. Coleman, Phys. Rev. B **29**, 3035 (1984).
- ³¹ G. Baym, L. P. Kadanoff, Phys. Rev. **124**, 287 (1961); G. Baym, Phys. Rev. **127**, 1391 (1962).
- ³² H. Keiter and J.C. Kimball, Int. J. Magn. **1**, 233 (1971) 233; N. Grewe and H. Keiter, Phys. Rev. B **24**, 4420 (1981).
- ³³ Y. Kuramoto, Z. Physik B **53**, 37 (1983).
- ³⁴ O. Sakai, M. Motizuki, and T. Kasuya, Springer Series in Solid-State Sciences **81**, 45 (Springer, 1988).
- ³⁵ Th. Pruschke and N. Grewe, Z. Phys. B **74**, 439 (1989).
- ³⁶ J. Holm and K. Schönhammer, Solid State Comm. **69**, 969 (1989).
- ³⁷ T.A. Costi, J. Kroha, and P. Wölfle, Phys. Rev. B **53**, 1850 (1996).
- ³⁸ K. Haule, S. Kirchner, J. Kroha, and P. Wölfle, Phys. Rev. B **64**, 155111 (2001).
- ³⁹ S. Kirchner and J. Kroha, J. Low Temp. Phys. **126**, 1233 (2002).
- ⁴⁰ J. Kroha and P. Wölfle, J. Phys. Soc. Japan **74**, 27 (2005).
- ⁴¹ A.A. Clerk and V. Ambegaokar, and S. Hershfield, Phys. Rev. B **61**, 3555 (2000).
- ⁴² N.E. Bickers and G.E. Zwicknagl, Phys. Rev. B **36**, 6746 (1987).
- ⁴³ L.S. Borkowski and P.J. Hirschfeld, J. Low Temp. Phys. **96**, 185 (1994).
- ⁴⁴ Y. Avishai, A. Golub, and A. D. Zaikin, Phys. Rev. B **63**, 134515 (2001).
- ⁴⁵ Y. Avishai, A. Golub, and A. D. Zaikin, Phys. Rev. B **67**, 041301 (2003).
- ⁴⁶ Y. Meir and N.S. Wingreen, Phys. Rev. Lett. **68**, 2512 (1992).
- ⁴⁷ A.V. Rozhkov and D.P. Arovas, Phys. Rev. Lett. **82**, 2788 (1999).
- ⁴⁸ F. Siano and R. Egger, Phys. Rev. Lett. **93**, 047002 (2004); err. Phys. Rev. Lett. **94**, 039902 (2005).
- ⁴⁹ M.-S. Choi, M. Lee, K. Kang, and W. Belzig, cond-mat/0410415.
- ⁵⁰ F. Siano and R. Egger, cond-mat/0410462.
- ⁵¹ P.W. Anderson, J. Phys. C **3**, 2436 (1970).
- ⁵² G. Sellier, PhD thesis, Univ. Karlsruhe 2002, *Quantum Impurities in Superconductors and Nanostructures: Selfconsistent Approximations and Renormalization Group Analysis* (Shaker Verlag, Aachen, 2003).
- ⁵³ K. Satori, H. Shiba, O. Sakai, and Y. Shimizu, J. Phys. Soc. Japan **61**, 3239 (1992).
- ⁵⁴ S. Elitzur, Phys. Rev. D **12**, 3978 (1975).
- ⁵⁵ J. Kroha, P. Wölfle, and T. A. Costi, Phys. Rev. Lett. **79**, 261 (1997).
- ⁵⁶ J. Kroha and P. Wölfle, Acta Phys. Pol. B **29**, 3781 (1998); J. Kroha and P. Wölfle, in *Theoretical Methods for Strongly Correlated Electrons*, CRM Series in Mathematical Physics, 297 (Springer, New York, 2003).